

Fluorescent and photo-oxidizing TimeSTAMP tags track protein fates in light and electron microscopy

Margaret T Butko¹, Jin Yang¹, Yang Geng^{2,3}, Hyung Joon Kim⁴, Noo Li Jeon⁴, Xiaokun Shu^{1,5,6}, Mason R Mackey^{7,8}, Mark H Ellisman^{7,8}, Roger Y Tsien¹ & Michael Z Lin¹⁻³

Protein synthesis is highly regulated throughout nervous system development, plasticity and regeneration. However, tracking the distributions of specific new protein species has not been possible in living neurons or at the ultrastructural level. Previously we created TimeSTAMP epitope tags, drug-controlled tags for immunohistochemical detection of specific new proteins synthesized at defined times. Here we extend TimeSTAMP to label new protein copies by fluorescence or photo-oxidation. Live microscopy of a fluorescent TimeSTAMP tag reveals that copies of the synaptic protein PSD95 are synthesized in response to local activation of growth factor and neurotransmitter receptors, and preferentially localize to stimulated synapses in rat neurons. Electron microscopy of a photo-oxidizing TimeSTAMP tag reveals new PSD95 at developing dendritic structures of immature neurons and at synapses in differentiated neurons. These results demonstrate the versatility of the TimeSTAMP approach for visualizing newly synthesized proteins in neurons.

Spatiotemporal control of protein synthesis is essential for proper development, normal functioning and adaptation of nervous systems. In embryonic neurons, proteins are synthesized in axonal growth cones during migration, and local inhibition of protein synthesis blocks growth-cone responses to axon guidance cues^{1,2}. Later in development, high levels of protein synthesis in dendrites and axons promote synapse formation^{3,4}. In the mature nervous system, protein synthesis is induced by neuronal activity and is required for memory consolidation in animals^{5,6}. Persistence of long-term potentiation (LTP) and long-term depression (LTD), activity-dependent changes in synaptic function believed to underlie learning, also requires new protein synthesis to persist beyond 1 h after induction^{7,8}. The production and targeting of new proteins also appears to be critical, as inhibition of protein synthesis locally at stimulated synapses blocks late-phase LTP at those synapses⁹.

The intricate regulation of protein synthesis during differentiation and plasticity of subcellular structures such as axons and synapses

suggests that those synthesized proteins are used in these structures. An attractive hypothesis for the function of activity-induced protein synthesis in memory formation is that new proteins incorporate into activated synapses, causing long-lasting changes in synaptic function¹⁰. However, which specific new protein species are locally incorporated during differentiation or plasticity and where they localize relative to subcellular structures undergoing change remains poorly understood¹⁰. An impediment to addressing these questions has been the lack of methods that can be generalized to visualize new copies of specific proteins in living cells and with subsynaptic spatial resolution.

We previously developed TimeSTAMP, a method for drug-controlled epitope tagging of newly synthesized proteins¹¹. In this method, a cassette comprising the nonstructural protein 3 (NS3), protease domain of hepatitis C virus (HCV) flanked by cognate protease sites is fused between a protein and an epitope tag. The protease excises itself and the tag from proteins by default, but this can be blocked for proteins synthesized after a defined time by applying a cell-permeant HCV NS3 protease inhibitor. These epitope-based TimeSTAMP tags have been used to visualize distributions of new proteins of interest in cultured mammalian neurons and in fly brains using immunostaining of fixed samples¹¹.

We now report an extension of the TimeSTAMP method to visualize new proteins in living cells by fluorescence microscopy and in fixed sections by high-resolution electron microscopy. Using a new fluorescent tag to track new copies of the protein PSD95, we find that local dendritic stimulation of growth factor and neurotransmitter receptors induces local accumulation of new PSD95 in stimulated synapses and dendritic shafts. Using new fluorescent photo-oxidizing tags, we show by correlated light and electron microscopy that newly synthesized PSD95 molecules rapidly incorporate beneath the postsynaptic membrane at synapses. The ability of these new TimeSTAMP tags to visualize new proteins in living neurons and at an ultrastructural level will enable researchers to study the role of new protein synthesis and delivery *in vitro* and *in vivo*.

¹Department of Pharmacology and Howard Hughes Medical Institute, University of California San Diego, La Jolla, California, USA. ²Department of Pediatrics, Stanford University, Palo Alto, California, USA. ³Department of Bioengineering, Stanford University, Palo Alto, California, USA. ⁴School of Mechanical and Aerospace Engineering, Seoul National University, Seoul, South Korea. ⁵Department of Pharmaceutical Chemistry, University of California San Francisco, San Francisco, California, USA. ⁶Cardiovascular Research Institute, University of California San Francisco, San Francisco, California, USA. ⁷National Center for Microscopy and Imaging Research, Center for Research on Biological Systems, University of California San Diego, La Jolla, California, USA. ⁸Department of Neurosciences, University of California San Diego, La Jolla, California, USA. Correspondence should be addressed to R.Y.T. (rtsien@ucsd.edu) or M.Z.L. (mzlin@stanford.edu).

Received 23 May; accepted 24 September; published online 28 October 2012; doi:10.1038/nn.3246

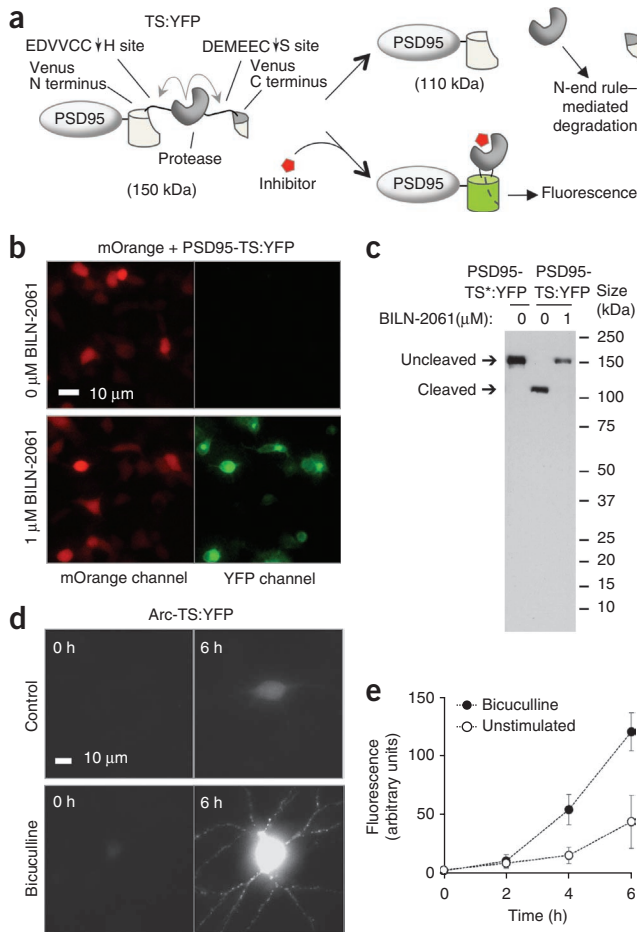


Figure 1 Development of TS:YFP, a TimeSTAMP tag with a YFP output. **(a)** Schematic of TS:YFP, which illustrates protease-mediated fragmentation of a fluorescent protein, fused to PSD95. **(b)** Micrographs of HEK293 cells without and with BILN-2061 continuously applied from 3 h after transfection to the time of imaging at 24 h after transfection with constructs expressing indicated proteins. **(c)** Immunoblots showing cleaved and full-length PSD95-TS:YFP fusion proteins in the absence of drug or with BILN-2061 continuously applied from 3 h after transfection to the time of lysis at 24 h after transfection. PSD95-TS*:YFP is a protease-dead mutant of PSD95-TS:YFP in which the serine of the catalytic triad is mutated to alanine. **(d)** Micrographs of 21-day *in vitro* (DIV) neurons transfected with Arc-TS:YFP constructs immediately before BILN-2061 addition and after 6 h in 1 μM BILN-2061 without (top) or with (bottom) exposure to 20 μM bicuculline simultaneously with BILN-2061. **(e)** Quantification of whole-cell Arc-TS:YFP fluorescence over time in unstimulated and stimulated neurons. Differences at 4 and 6 h are significant ($P < 0.05$ by unpaired two-sided *t*-test, $n = 6$ neurons per condition). Error bars, s.e.m.

tagging in neurons and had no effect on synaptogenesis when targeted to synapses via PSD95 (Supplementary Fig. 1g,h).

We next used TimeSTAMP2 to create autofluorescent drug-controlled labels of new protein copies. We screened insertions of the TimeSTAMP and TimeSTAMP2 modules into loops of fluorescent protein domains for drug-dependent fluorophore development. Among the constructs tested (Supplementary Fig. 2a), the Venus yellow fluorescent protein with the TimeSTAMP2 module inserted between amino acids 158 and 159 exhibited robust drug-dependent fluorescence (named TS:YFP; Fig. 1b). Immunoblotting confirmed that protease excision occurred efficiently in the absence of the drug but was fully inhibited in the presence of 1 μM BILN-2061 (Fig. 1c). The fusion of this construct to PSD95 localized to synapses similarly to the previously characterized PSD95-CFP¹² (Supplementary Fig. 2b), and it did not exert observable effects on synaptogenesis (Supplementary Fig. 2c). Therefore, this construct, TimeSTAMP:YFP (TS:YFP), can function as a drug-inducible continuous fluorescent label of newly synthesized proteins.

TS:YFP fluorescence arising during drug treatment persisted after drug washout (Supplementary Fig. 2d), consistent with previous findings that fluorescent protein fragment assembly is irreversible¹³. Thus, TS:YFP should function for pulse labeling by irreversibly labeling proteins synthesized in a drug-defined pulse period that is followed by production of unlabeled protein after washout. This would be conceptually analogous to pulse-chase labeling with radioactive metabolic precursors, without requiring a ‘chase’ with excess non-radioactive precursors to dilute radioactive precursors. To test optical pulse labeling, we expressed in primary rat embryonic hippocampal neurons the transmembrane synaptic adhesion molecule Neuroligin3 (NLGN3) tagged with TS:YFP. At 14 d *in vitro* (DIV), we induced fluorescence on new proteins by incubation with the drug for 18 h followed by washout of the drug. Time-lapse microscopy showed fluorescence appearing during the pulse period, initially in perinuclear structures consistent with endoplasmic reticulum and Golgi and then at the cellular membrane and in synapses (Supplementary Fig. 2e). After washout of the drug, fluorescence decreased in all locations with an approximate half-life of 24 h, consistent with half-life measurements performed by isotope labeling¹⁴. These results confirm that TS:YFP can be used for optical pulse labeling.

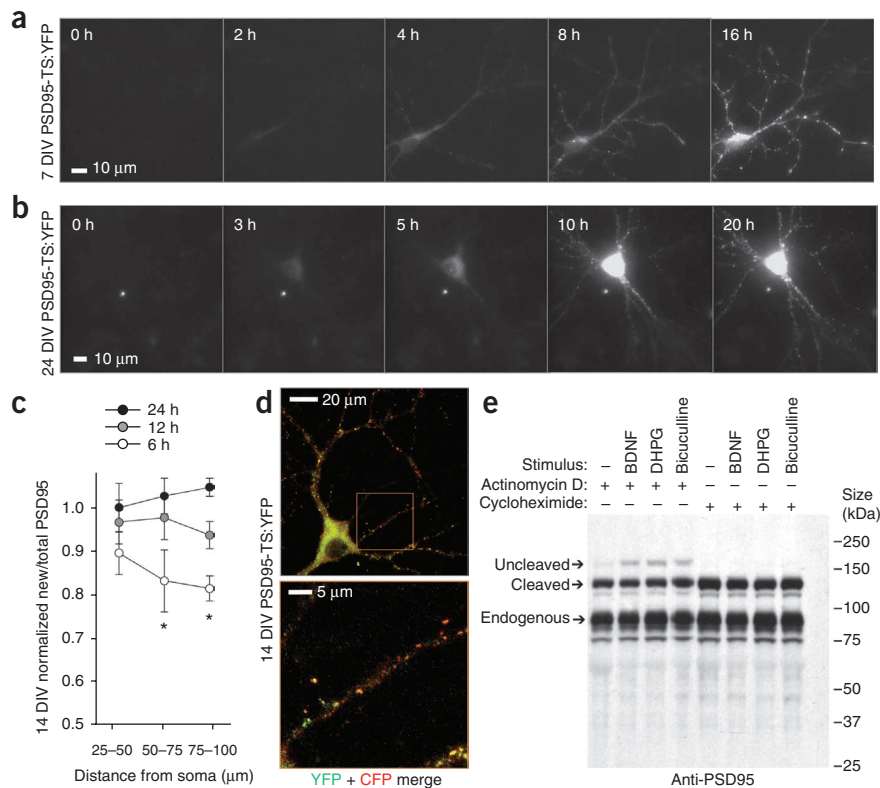
To test the capability of TS:YFP to report on activity-dependent protein synthesis, we tracked the production of Arc, which is translationally induced by synaptic activity⁸, in basal and stimulated conditions. For this reporter, we fused the TS:YFP coding sequence 3’ to the Arc coding sequence and included the complete pre-mRNA sequence with the 3’ untranslated region (UTR) and introns, which

RESULTS

Development of fluorescent TimeSTAMPs

To track newly synthesized proteins of interest in living neurons, we first extended the TimeSTAMP technique to control maturation of fluorescent protein domains with a drug. We reasoned that the NS3 protease placed within a fluorescent protein domain and allowed to remove itself in the absence of the drug would generate fluorescent protein fragments that do not associate and do not produce fluorescence, whereas protease inhibition resulting from application of the drug would preserve linkage, allowing for fluorophore maturation (Fig. 1a). We first generated a single TimeSTAMP cassette to improve signal inducibility and to induce degradation of the protease after self-excision (Supplementary Fig. 1a). We improved cleavage efficiency and inhibitor binding by fusing the 8-amino-acid NS4A beta strand cofactor N-terminally to the NS3 domain. Breakthrough cleavage in the presence of the drug was reduced by introducing the slow-cleaving T54A mutation into NS3 (ref. 11). We achieved inducible protease excision and elimination by introducing a new N-terminal *cis*-linked cleavage site with the P6–P1 sequence EDVVCC derived from the naturally preferred NS5A/NS5B cleavage substrate and with the N-end rule-inducing histidine at the P1’ position. The resulting cassette, TimeSTAMP2, showed improved control by NS3 protease inhibitors (complete inhibition at 1 μM BILN-2061 or ITMN-191 compared to 10 μM for original TimeSTAMP, Supplementary Fig. 1b,c). As desired, protease did not accumulate in the absence of the drug (Supplementary Fig. 1d–f). Similar to the original TimeSTAMP tags, TimeSTAMP2 allowed drug-dependent epitope

Figure 2 Tracking of basal and activity-induced PSD95 production with TimeSTAMP. **(a,b)** Time-lapse images of 7-DIV **(a)** and 24-DIV **(b)** neurons expressing PSD95-TS:YFP constructs incubated with BILN-2061 for the indicated durations. **(c)** In 14-DIV neurons, PSD95-TS:YFP fluorescence in segments of the primary dendrite divided by PSD95-CFP fluorescence for each time and then normalized to the initial value in the 25- μ m segment. Mean differences between times were significant for 50–75 μ m and 75–100 μ m segments by ANOVA ($P = 0.018$ and $P = 0.020$, respectively; $n = 7$ segments each). Differences between 24 h and 6 h were significant by post-hoc Tukey's tests ($P = 0.017$ and $P = 0.016$ for segments at 50–75 μ m and 75–100 μ m, respectively). Error bars, s.e.m. **(d)** Micrograph of a representative neuron from **c** exposed for 20 h to 1 μ M BILN-2061 under basal conditions (top). PSD95-TS:YFP protein is in green, and PSD95-CFP, a marker of total PSD95, is in red. Magnification of the boxed region in top image (bottom). **(e)** Anti-PSD95 immunoblotting for 14-DIV neurons expressing PSD95-GFP-TimeSTAMPa treated for 3 h with 10 μ M BILN-2061 and indicated stimuli along with actinomycin D to block transcriptional upregulation or cycloheximide to block protein synthesis 100 ng ml⁻¹ BDNF, 50 μ M DHPG and 20 μ M bicuculline each induced PSD95 synthesis above baseline independent of transcription. Endogenous PSD95 served as a loading control.



are involved in *Arc* mRNA localization and translational induction by neuronal activity¹⁵. In 21-DIV hippocampal neurons expressing this Arc-TS:YFP reporter, no fluorescence was detectable from the transfected neurons before BILN-2061 treatment, whereas fluorescence increased over time in 1 μ M BILN-2061 (Fig. 1d). Bicuculline, which promotes generation of action potentials in excitatory glutamatergic neurons by antagonizing GABA receptors, increased the rate of fluorescence development (Fig. 1e), consistent with previous observations¹⁶, thereby confirming that TS:YFP can report activity-dependent protein translation.

To simultaneously visualize newly synthesized proteins from two species, we also created an orange fluorescent protein TimeSTAMP (TS:OPF) using a different design based on cleavage-induced N-end rule degradation of a fully intact mKO2 orange fluorescent protein (Supplementary Fig. 3a). In the absence of a drug, the released protease-mKO2 fusion was degraded, as assessed by direct fluorescence and immunoblotting (Supplementary Fig. 3b,c), whereas EGFP, mCherry or Venus in place of mKO2 were resistant to degradation (Supplementary Fig. 3d). This TS:OPF tag may be useful together with TS:YFP for tracking new copies of two proteins simultaneously. However, one clear advantage of TS:YFP is that the fluorescent protein remains intact after drug washout for monitoring protein turnover by fluorescence.

Stimulus-dependent PSD95 translation revealed by TimeSTAMP

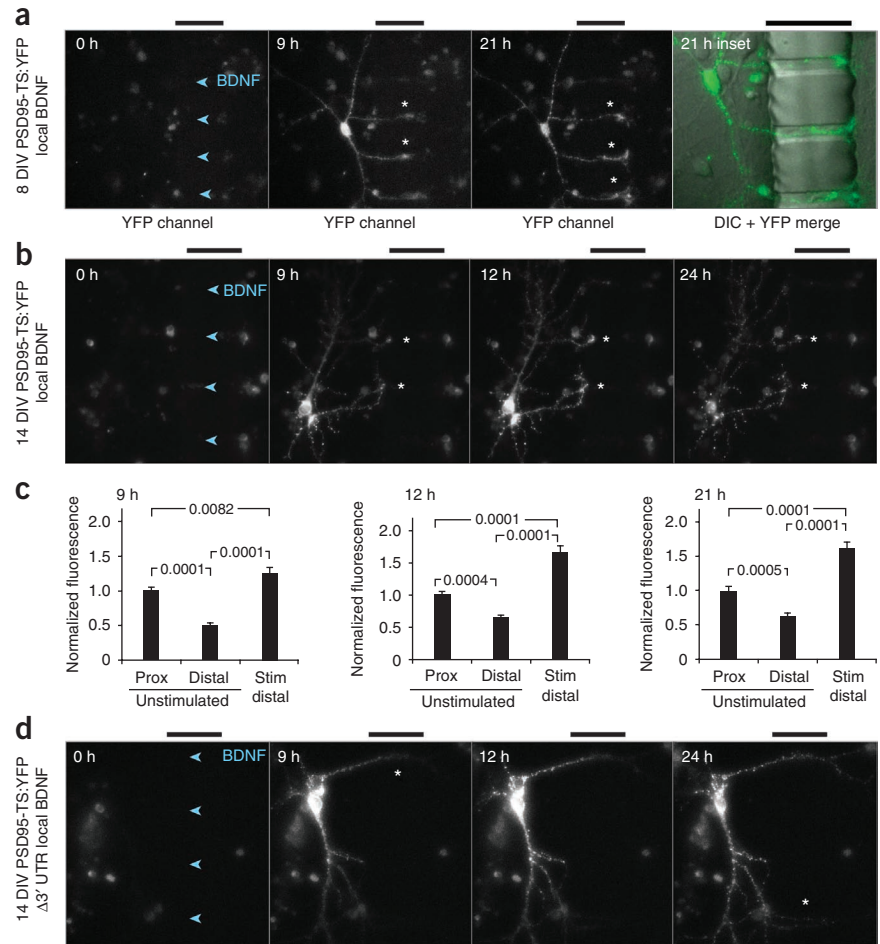
We next used fluorescent TimeSTAMP to test whether synaptic proteins synthesized after induction of plasticity incorporate into stimulated synapses. It has been suggested that activity-induced proteins are delivered to stimulated synapses to promote the persistence of plasticity. PSD95 functions to build a postsynaptic density (PSD) by cross-linking receptors and cytoskeletal elements¹⁷, and its synthesis is

induced in synaptoneurosomes by stimulation of metabotropic glutamate receptor (mGluR)¹⁸. However, whether local stimulation induces local synaptic accumulation of new PSD95 has not been investigated.

To visualize new PSD95 in living neurons, we fused PSD95 coding sequence to that of TS:YFP and included the complete native 3' UTR, required for mRNA stabilization and translational control^{18–20}. Neurons expressing this PSD95-TS:YFP reporter exhibited no fluorescence in the absence of BILN-2061, but fluorescence accumulated over time in its presence (Fig. 2a). Neurons expressing this construct and undergoing synaptogenesis at 7 DIV showed drug-dependent fluorescence in dendritic puncta that appeared simultaneously with dendrite arborization (Fig. 2a), suggesting incorporation of new PSD95-TS:YFP into nascent synapses as previously observed with TimeSTAMP tags¹¹. At 24 DIV, drug-dependent fluorescence arose gradually over 24 h in puncta throughout the dendritic tree, consistent with accumulation at preexisting synapses (Fig. 2b). Similarly, ratios of new/total PSD95 in neurons at 14 DIV revealed slower synaptic accumulation of newly synthesized PSD95-TS:YFP further from the cell body, as indicated by ratios of PSD95-TS:YFP/PSD95-CFP fluorescence (Fig. 2c,d), similar to earlier observations¹¹. These results confirm that TS:YFP can track new copies of PSD95 and that under basal conditions new PSD95 expression does not occur preferentially in dendrites.

We next investigated the regulation of PSD95 translation in experimental models of synaptic plasticity. The TrkB receptor tyrosine kinase and type 1 mGluRs regulate protein synthesis in synaptic plasticity, and TrkB activation by brain-derived neurotrophic factor (BDNF) is both necessary for the late phase of electrically induced LTP²¹ and sufficient to induce long-lasting increases in synaptic currents that resemble electrically induced LTP²². Activation of type 1 mGluRs

Figure 3 BDNF-dependent local accumulation of new PSD95 in neurons. **(a,b)** Time-lapse images of 8-DIV **(a)** and 14-DIV **(b)** neurons expressing PSD95-TS:YFP treated with 1 μM BILN-2061 in both chambers and 100 ng ml^{-1} BDNF in the right chamber of a microfluidic device for the indicated durations. Arrowheads in the channels point in the direction of BDNF diffusion, and bars above the images mark the location of the 50- μm barrier. Asterisks mark growth cones with new PSD95 **(a)** or distal dendritic enrichment of new PSD95 **(b)**. The 21 h inset in **a** shows merged TS:YFP fluorescence (green) and differential interference contrast (DIC, grayscale) images. **(c)** New PSD95 mean concentrations in synapses of stimulated regions (within 10 μm of the microchannels, $n = 31$) versus synapses located more proximally on the same dendritic branch ($n = 40$ synapses) as well as versus synapses equidistant from the soma on an unstimulated branch ($n = 36$ synapses). Differences were significant by one-way ANOVA at all time points ($P = 0.0001$). P values of post-hoc unpaired two-tailed t -tests with Tukey's correction are indicated. Error bars, s.e.m. **(d)** Fluorescence images as in **a,b** of neurons expressing a construct lacking the 3' UTR. Asterisks indicate a proximal-distal gradient of PSD95 along a dendrite.



by pharmacological agonists CHPG and DHPG can either induce LTD or decrease stimulation thresholds for LTP, depending on the context²³. Both receptor classes activate the PI3K-mTOR pathway^{24,25}, which can promote PSD95 translation²⁶. To determine whether TrkB or type 1 mGluR pathways regulate PSD95 translation, we performed immunoblotting experiments with PSD95-GFP-TimeSTAMPA, composed of PSD95 fused to GFP and TimeSTAMPA, with the cassette encoding the complete 3' UTR of the gene encoding PSD95 (ref. 11). Bath stimulation of 14-DIV neurons with BDNF or the type I mGluR agonist DHPG increased the amount of new PSD95-GFP, detected as a slower migrating species in the presence of BILN-2061 (Fig. 2e). This induction was blocked by cycloheximide but was insensitive to actinomycin D, indicating dependence on protein synthesis but not on transcription. Bicuculline also enhanced new PSD95-GFP protein production. These results indicate that PSD95 synthesis is regulated by neurotrophin and neurotransmitter receptors and by synaptic activity.

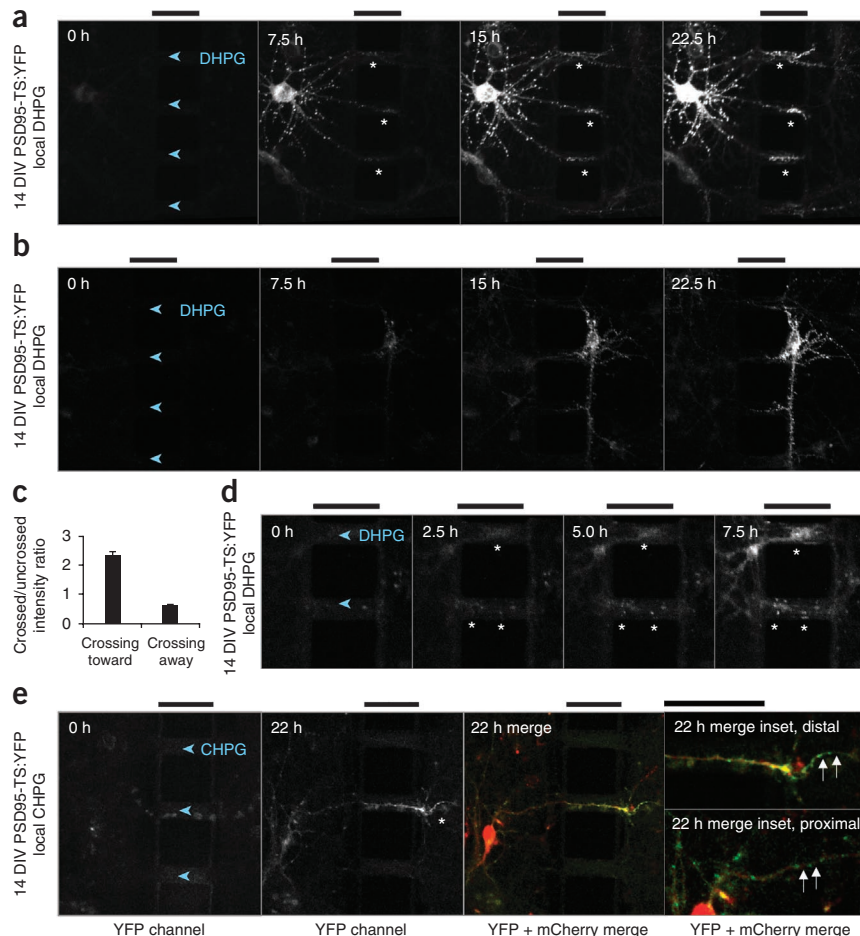
We next hypothesized that TrkB or type 1 mGluR activation can induce local accumulation of new PSD95 at stimulated dendritic regions and synapses. To perform local stimulations, we microfabricated polydimethylsiloxane devices in which two culture compartments were separated by a 50- μm -thick barrier traversed by 7- μm -wide microchannels connecting the compartments (Supplementary Fig. 4a). This device is based on earlier devices for axonal isolation²⁷, but the barrier is thinner to permit dendrites to traverse. Compounds applied to one compartment diffuse down the microchannels, but compound concentrations in both compartments do not detectably change over 12 h even without active microfluidic control owing to the small volumes of the microchannels compared to those of the compartments (Supplementary Fig. 4b-d). When we transfected neurons and plated them in both compartments, some neurons extended their dendrites through the

microchannels to the opposite compartment, allowing their distal dendrites to be selectively stimulated (Supplementary Fig. 4e).

Specificity of new PSD95 for stimulated synapses

To determine whether distributions of new PSD95 copies can be spatially regulated in developing neurons, we stimulated distal dendrites of 8-DIV neurons expressing PSD95-TS:YFP with BDNF and added BILN-2061 to both chambers to monitor new PSD95 anywhere. New PSD95 copies were enriched at tips of neurites extending toward the BDNF-stimulated compartment in the microchannels (Fig. 3a). These structures are likely developing dendrites rather than axons because there were several of them, and because of their thickness and the presence of PSD95. Fluorescence intensity per dendritic length was higher in BDNF-stimulated distal segments than in proximal segments of the same dendrite and higher in stimulated dendritic segments than in segments from matched unstimulated dendrites equally far from the cell body (Fig. 3a). To determine whether new PSD95 protein can preferentially accumulate in stimulated synapses in response to BDNF, we performed this experiment in 14-DIV neurons. Local BDNF stimulation induced intense accumulations of new PSD95 in shafts and synapses of dendrites entering the microchannels beginning at 9 h and persisting to 24 h after drug application (Fig. 3b). At 9 h, 12 h and 21 h, synaptic intensities of new PSD95 (adjusted for synapse size) in stimulated distal regions were 26–62% higher than in unstimulated proximal regions of the same dendrite and 121–153% higher than in unstimulated distal regions of dendrites from the same cell that were similarly distant from the cell body (Fig. 3c). These results

Figure 4 Local new PSD95 accumulation is induced by local metabotropic glutamate receptor activation. **(a)** Time-lapse imaging of a 14-DIV neuron in the presence of 1 μ M BILN-2061 in both chambers and 100 μ M DHPG in the right chamber of a microfluidics device for the indicated durations. Asterisks indicate enrichment of new PSD95. **(b)** Images of a representative neuron exhibiting no enrichment of new PSD95 in distal dendrites crossing from the DHPG-stimulated compartment into the unstimulated compartment. **(c)** Mean ratio of new PSD95 in synapses in a 20- μ m dendritic segment crossing the barrier versus in a 20- μ m noncrossing dendritic segment from the same neuron, quantified at 22.5 h. This ratio was greater than 1 in neurons with cell bodies in the unstimulated compartment extending dendrites into the stimulated compartment, but less than 1 for neurons extending dendrites in the opposite direction ($P = 0.009$ by unpaired two-tailed *t*-test, $n = 8$ and $n = 4$ segments for crossing-toward and crossing-away neurons, respectively). Error bars, s.e.m. **(d)** Enrichment of new PSD95 in synapses and dendrites encountering DHPG (asterisks) detectable at early time points. **(e)** Enrichment of new PSD95 (asterisk) in stimulated dendrites in response to 300 μ M of the mGluR5-selective agonist CHPG. The 22 h merge shows TS:YFP (green) and mCherry (red) signals. In the magnified insets, new PSD95 is seen in the dendritic shaft in the stimulated region (top) but not in the unstimulated region (bottom). The intensity gain of the TS:YFP signal in the bottom inset is twice that of the other images. In all images, arrowheads in the channels point in the direction of DHPG or CHPG diffusion, and bars above the images mark the 50- μ m barrier.



reveal that new PSD95 copies can be preferentially expressed at BDNF-stimulated dendritic regions and synapses.

The reporter constructs used in the above experiments included the complete 3' UTR of the gene encoding PSD95, which mediates localization of the mRNA to dendrites and translational regulation by FMRP^{18,20}. Removal of the 3' UTR would be expected to prevent dendritic localization of the mRNA and FMRP-dependent translational induction, and this truncation would test whether local BDNF-induced signals recruit PSD95 proteins synthesized in an FMRP-independent manner in the cell body. In neurons expressing PSD95-TS:YFP lacking the 3' UTR and dendritically stimulated with BDNF, new PSD95 was primarily expressed in the cell body with no specific enrichment in stimulated regions at any time (Fig. 3d). These results indicate that dendritic translation of PSD95 and/or FMRP involvement is required for localized dendritic accumulation of new PSD95 at stimulated synapses, and they demonstrate that TS:YFP can be used to study 3' UTR function in mediating activity-dependent local accumulation of new synaptic proteins.

To determine whether new PSD95 proteins are also recruited to synapses after mGluR stimulation, we stimulated distal dendrites of 14-DIV neurons expressing PSD95-TS:YFP with DHPG. We again observed synaptic accumulation of new PSD95 in stimulated regions (Fig. 4a and Supplementary Videos 1 and 2). By contrast, dendrites extending toward the unstimulated side showed less new PSD95 (Fig. 4b), ruling out that the effect is a nonspecific result of crossing through a microchannel. New PSD95 was enriched 2.4-fold in stimulated segments compared to unstimulated segments equidistant from

the cell body at 22.5 h (Fig. 4c); the magnitude of this enrichment was similar to increased levels of translationally regulated protein that had been previously observed with neurotransmitter receptor modulation^{28,29} and cannot be accounted for solely by the 20% increase in PSD size previously observed in response to BDNF³⁰. In some neurons, new PSD95 enrichment was first visible in stimulated synapses 2.5 h after stimulation began (Fig. 4d) and persisted for the duration of the experiment. We obtained similar results with CHPG, a specific agonist of mGluR5, the predominant type 1 mGluR at hippocampal synapses³¹ (Fig. 4e). Close examination revealed that new PSD95 was present in both synapses and dendritic shafts in the stimulated region (Fig. 4a,e). These findings show that neurotransmitter receptor activation in a dendritic region can induce accumulation of new copies of PSD95 in the stimulated region, including at synapses. These results demonstrate the use of TS:YFP to visualize new copies of a synaptic protein during local dendritic stimulations.

Development of photo-oxidizing TimeSTAMPS

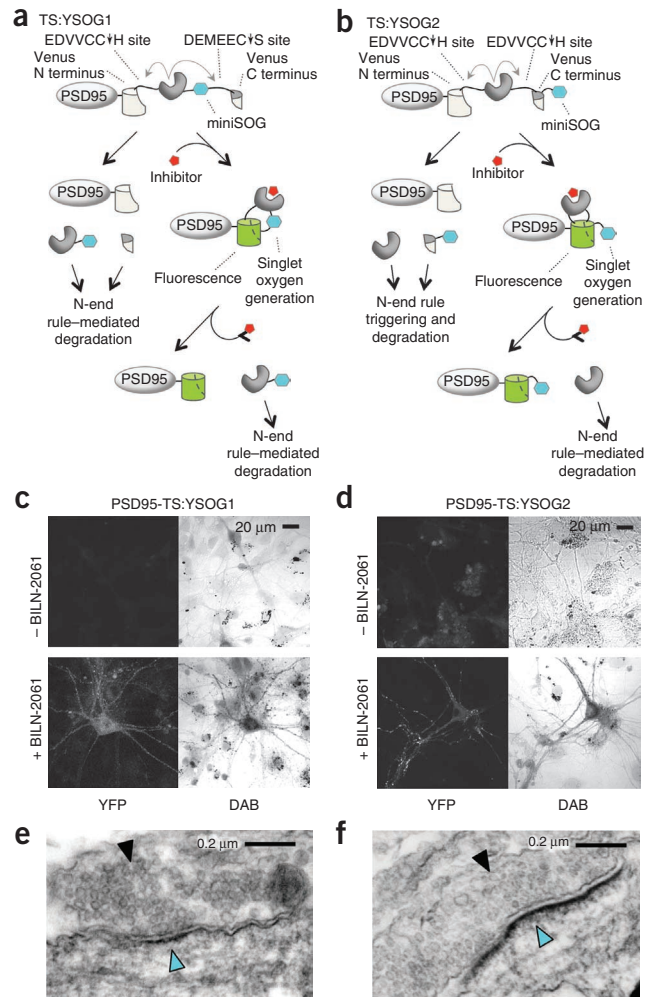
We next sought to visualize new proteins of interest in neurons with ultrastructural resolution by electron microscopy. Because two epitope tags in TS:YFP are drug-dependent (Supplementary Fig. 5a–e), we first tested peroxidase-conjugated antibodies to deposit diaminobenzidine (DAB) for electron microscopy imaging. However, the permeabilization steps required for antibody penetration resulted in poor ultrastructural detail (Supplementary Fig. 5f). Therefore, we modified TS:YFP to add the 12-kDa genetically encoded singlet oxygen generator miniSOG, which can mediate photo-oxidation of

Figure 5 Design and development of photo-oxidizing TimeSTAMPs. **(a,b)** Schematics of TS:YOG1 **(a)** and TS:YOG2 **(b)** cassettes with a drug-dependent capacity to generate singlet oxygen encoded by the miniSOG domain (cyan), fused to the synaptic protein PSD95. **(c,d)** Fluorescence and DAB images of neurons expressing PSD95-TS:YOG1 **(c)** and PSD95-TS:YOG2 **(d)** showing drug-dependent signals. **(e,f)** Images show PSD95-TS:YOG1 **(e)** and PSD95-TS:YOG2 **(f)** DAB signal localized to PSDs of neurons incubated with drug. Solid arrowhead marks abundant 30–40-nm vesicles indicative of a presynaptic bouton. Cyan arrowhead indicates DAB signal at and beneath the apposing postsynaptic membrane. The excess black dots present in transmitted light images in **c** and **d** are nonspecific miniSOG-independent DAB precipitates that commonly form when photo-oxidizing cultured neurons. Because this signal is mainly extracellular and does not match YFP fluorescence, it was easily distinguishable from true miniSOG signal at transmitted light and electron microscopy levels.

DAB for electron microscopy visualization³². Photo-oxidation with miniSOG removes concerns about nonspecific antibody binding and does not require sample permeabilization, allowing for better ultrastructural preservation³². We created two designs incorporating miniSOG (Fig. 5a,b). In TimeSTAMP:YFPminiSOG 1 (TS:YOG1), we fused miniSOG to the protease domain in TS:YFP for degradation by the N-end rule in the absence of the drug but preservation in its presence (Fig. 5a). In TS:YOG2, we fused miniSOG after the C-terminal YFP fragment and changed the C-terminal cleavage sequence to allow for cleavage-induced N-end rule-mediated degradation of miniSOG in the absence of the drug but preservation in its presence (Fig. 5b). Although the second version is limited by fusion to the C terminus of proteins of interest because it degrades its C-terminal cleavage product, its advantage over the first is its applicability for pulse labeling. Because miniSOG in TS:YOG2 is covalently linked to the C-terminal YFP fragment, it will remain bound to the protein of interest during the drug pulse and the drug washout (Fig. 5b), whereas miniSOG in TS:YOG1 would be cleaved away and degraded with the protease during the drug washout (Fig. 5a).

In lysates from cells expressing PSD95-TS:YOG1 or PSD95-TS:YOG2 grown without BILN-2061, blotting for the AU1 (DTYRYI) or hemagglutinin (HA) epitope tag, respectively, in the miniSOG fragment revealed no protein (Supplementary Fig. 6a,b), confirming efficient cleavage and N-end rule-mediated degradation. In the continual presence of BILN-2061, we detected only uncleaved PSD95-TS:YOG1 or PSD95-TS:YOG2, respectively, as expected. Both constructs exhibited fluorescence induction by BILN-2061 similar to the case for TS:YFP (Supplementary Fig. 6c). Like PSD95-TS:YFP, PSD95-TS:YOG1 and PSD95-TS:YOG2 both localized to synaptic sites on dendritic spines without disrupting synaptogenesis (Supplementary Fig. 6d–f).

We tested the performance of photo-oxidizing TimeSTAMP tags in correlated light and electron microscopy. In 12-DIV neurons expressing PSD95-TS:YOG1 or PSD95-TS:YOG2, fluorescence was negligible in the absence of the drug but appeared throughout cells after 48 h with the drug (Fig. 5c,d). We fixed these neurons without permeabilization and performed miniSOG-dependent photo-oxidation of DAB with blue light. The resulting DAB precipitate overlapped well with the YFP signal by light microscopy, indicating specificity for the reporter protein (Fig. 5c). By electron microscopy, fine subcellular structures such as microtubules and synaptic vesicles were clearly visible in photo-oxidized samples (Fig. 5e,f), demonstrating excellent preservation of ultrastructure and fine resolution of synaptic elements similar to the case with conventional label-free samples³³. The majority of the DAB label localized to submembrane locations across from synaptic vesicles, consistent with PSD95 localization, and DAB signal was dependent on the presence of the drug (Supplementary Fig. 7a,b).

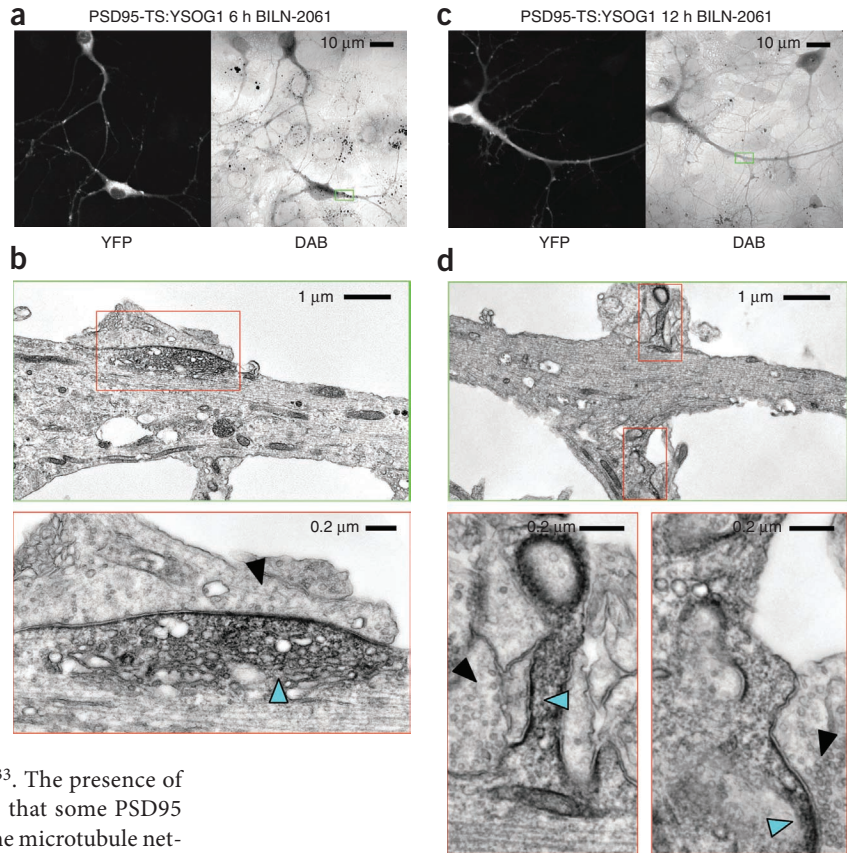


In early experiments, miniSOG-independent DAB signal appeared in neuronal mitochondria after photo-oxidation (Supplementary Fig. 8a). Endogenous mitochondrial iron-sulfur complexes can photosensitize oxygen at the wavelengths used with miniSOG, but mersalyl acid abolishes this effect²⁸. Indeed, mersalyl acid treatment (5 mM, 30 min) before photo-oxidation reduced mitochondrial DAB signal eightfold (Supplementary Fig. 8b,c). With this step included, electron microscopy of DAB-positive puncta in neurons expressing PSD95 tagged with either TS:YOG1 or TS:YOG2 reliably revealed synaptic structures with excellent ultrastructural preservation and with the highest electron density under the postsynaptic membrane, as expected (Supplementary Fig. 8d,e). These results confirm that photo-oxidizing TimeSTAMP tags allow high-resolution electron microscopy imaging.

Tracking labeled PSD95 copies with subsynaptic resolution

We examined distributions of freshly synthesized PSD95 using TS:YOG1 by treating neurons expressing PSD95-TS:YOG1 at 12 DIV, a time of synaptogenesis, with 1 μM BILN-2061 for 6 h before fixation. By fluorescence microscopy, YFP signal appeared diffusely throughout the dendrite except for a few large puncta (Fig. 6a). These puncta appeared larger than typical PSDs, but the resolution of fluorescence microscopy was insufficient to determine if they contain synapses. We then performed photo-oxidation and obtained a pattern of DAB deposition similar to that of YFP fluorescence. Electron microscopy visualization of one dendritic PSD95 accumulation

Figure 6 Tracking new PSD95 populations using TS:YSG1. (a) Images of neurons after 6 h in BILN-2061, showing new PSD95 protein throughout shafts with enrichment in 2 μm -wide accumulations. (b) Electron microscopy imaging of one accumulation after photo-oxidation revealed a diffuse accumulation of membrane-bound and cytoplasmic PSD95 (cyan arrowhead) in contact with an axonal region with a low density of vesicles (solid arrowhead). (c) Images of neurons after 12 h in BILN-2061, showing new PSD95 protein throughout shafts and in many puncta less than 1 μm wide. (d) Electron microscopy imaging of two small puncta revealed membranous and submembranous PSD95 (cyan arrowheads) in contact with an axonal region with high vesicular density indicative of a mature synapse (solid arrowheads).



located at a junction with an axon in the fluorescence image (Fig. 6a) revealed it to be in a dendritic protrusion and containing diffuse DAB signal (Fig. 6b). There was little signal in the rest of the dendrite, suggesting that new PSD95 preferentially localized to these diffuse accumulations (Fig. 6b). This accumulation was 2 μm wide and 0.6 μm deep, larger in each axis than a mature PSD³³. The presence of PSD95 that is not membrane-associated implies that some PSD95 protein may not be palmitoylated³⁴. In addition, the microtubule network appeared disorganized in this protrusion, suggesting that this was a dynamic structure in the cell³⁵. This protrusion was apposed to an axonal segment with a low density of vesicles (fewer than four within 100 nm), a criterion used to describe immature synapses under electron microscopy³⁶. We speculate that this structure may be a newly forming synapse, as new synapses often arise at sites with diffuse accumulations of PSD95 (refs. 11,37).

In PSD95-TS:YSG1-expressing neurons treated with BILN-2061 for 12 h, we observed labeling of new PSD95 throughout dendrites by both fluorescence microscopy and DAB staining (Fig. 6c). In one region examined by electron microscopy, we observed the

highest signal in spines, and new PSD95 preferentially accumulated on membranes contacting apposing mature presynaptic structures (Fig. 6c,d). These accumulations measured 500 nm wide and less than 30 nm deep, dimensions typical for a mature PSD³³. Thus, new PSD95 populations appear at mature synapses within 12 h.

To pulse-label PSD95 synthesized in a specific time window, we incubated 12-DIV neurons expressing PSD95-TS:YSG2 with 1 μM BILN-2061 for 48 h and then removed the drug for 6 h. By fluorescence microscopy, we observed YFP signal in small and bright puncta in distal neuronal processes (Fig. 7a). We also noticed a decrease in

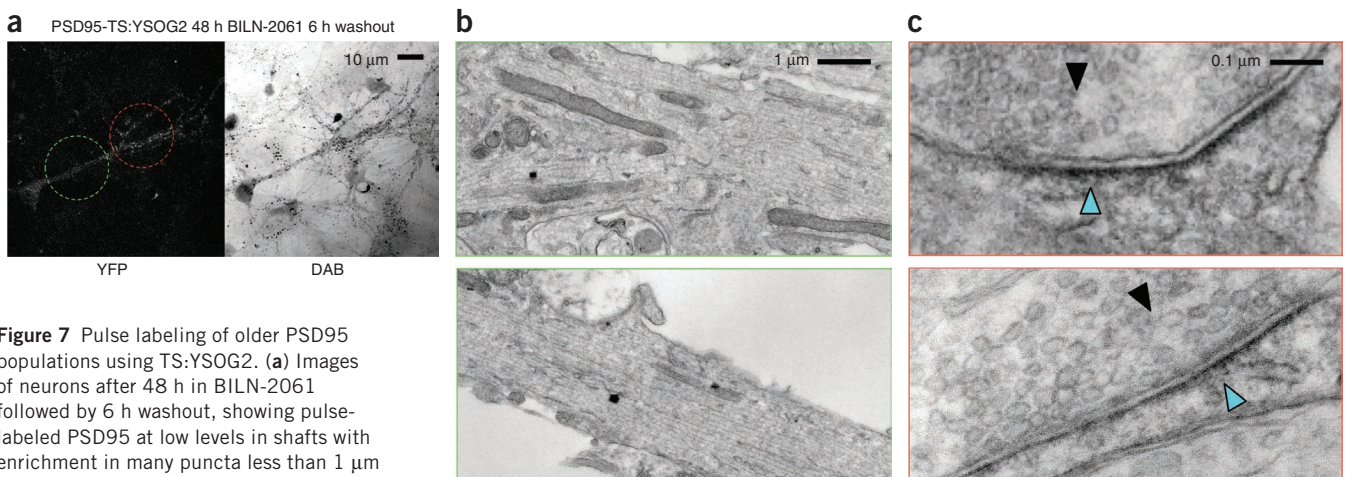


Figure 7 Pulse labeling of older PSD95 populations using TS:YSG2. (a) Images of neurons after 48 h in BILN-2061 followed by 6 h washout, showing pulse-labeled PSD95 at low levels in shafts with enrichment in many puncta less than 1 μm wide. (b) Electron microscopy imaging in a dendritic shaft area without fluorescent puncta (green dashed circle in a) showing no accumulations of pulse-labeled PSD95. (c) Electron microscopy imaging in an area with fluorescent puncta (red dashed circle in a) showing pulse-labeled PSD95 at multiple synapses, detected as membrane-bound aggregations of 500 nm width (cyan arrowheads) facing a presynaptic zone with many synaptic vesicles (solid arrowheads).

diffuse YFP signal in soma and proximal processes compared to neurons maintained continuously in drug (Fig. 6b and 7a), suggesting that proteins labeled in the pulse period have moved out of these structures. After photo-oxidation, we visualized by electron microscopy two dendritic areas in one cell (Fig. 7a). A more proximal area that had only dim diffuse signal by fluorescence microscopy exhibited no specific DAB signal by electron microscopy, suggesting clearance of PSD95 proteins from the cytosol 6 h after synthesis (Fig. 7b). A more distal area containing multiple fluorescent puncta smaller than 1 μm in diameter exhibited PSD95 proteins localized to mature synapses, as indicated by submembranous staining apposing pre-synaptic structures with abundant vesicles (Fig. 7c). Taken together, these results show that new PSD95 proteins localize to synapses by 6 h after synthesis in 14-DIV neurons.

DISCUSSION

Comparison of TimeSTAMPs with other translation reporters

The TimeSTAMP tags we developed have a unique combination of features suitable for studying the fates of newly synthesized proteins during nervous system development and plasticity. First, they are genetically encoded, so they can be appended to specific proteins of interest. Second, they are drug-controllable, which both provides an easy means to control the time period of new protein labeling and enables control in large tissue volumes. Last, they are fluorescent and photo-oxidizing, allowing visualization of new protein copies in living cells and by electron microscopy.

As protein tags, TimeSTAMPs can report on all steps that control protein expression and localization, including transcriptional, translational and post-translational regulatory events and protein-protein interactions. This is especially critical for studying synaptic proteins, which are dynamically regulated by multiple mechanisms. For instance, proteins of the PSD are held together by a network of protein-protein interactions, which are regulated by post-translational modifications such as phosphorylation³⁸, palmitoylation³⁹, proteolysis⁴⁰ and ubiquitination⁴¹. In contrast, destabilized GFP reporters cannot be used as fusion tags because of their destabilizing nature, and although they can report on transcriptional and translational control^{28,29}, they do not report on subsequent steps of protein localization, interactions or modification.

Monomeric fluorescent protein timers and photoconvertible fluorescent proteins⁴² can in theory be used as fluorescent tags that report on protein age in living cells. However, a population of timer molecules changes color gradually over many hours owing to an autocatalytic conversion reaction occurring at different times in each molecule, and thus fluorescent protein timers cannot provide the same temporal resolution or control as TimeSTAMP⁴². Monomeric photoconvertible fluorescent proteins can be fused to a protein of interest and converted from one emission wavelength to another using violet light⁴², after which only new proteins will fluoresce at the unconverted wavelength. However, detecting low concentrations of new proteins requires complete conversion throughout the cell, and the required prolonged exposures and high intensities often cause phototoxicity⁴³. Extending the use of photoconvertible proteins to a large volume *in vivo* would also be difficult, whereas drugs are routinely perfused throughout a slice or injected into a brain region.

A powerful nongenetic approach to label new proteins is to metabolically incorporate physically or chemically distinct amino acids. Classically this has been performed with radioactive amino acids for detection by autoradiography. Recently the approach has been extended to amino acids with nonradioactive isotopes for detection by mass spectroscopy and, in the bioorthogonal noncanonical

amino acid tagging (BONCAT) technique, to unnatural amino acids containing reactive chemical groups that can then be conjugated to fluorophores or affinity tags⁴⁴. These metabolic labeling approaches differ in applicability from TimeSTAMP in two ways. First, they result in the labeling of all new proteins proportional to abundance rather than specifically labeling proteins of interest. Second, they currently do not allow live visualization of new proteins. For visualization with autoradiography, samples must be fixed and then exposed to film. For visualization with BONCAT, cells must be starved of natural amino acids before addition of unnatural amino acids, then after the labeling period, fixed and reacted in nonphysiological conditions. Metabolic labeling approaches, however, enable *de novo* identification of synthesized proteins, either by mass spectrometry for heavy isotopes or by reaction to affinity groups and purification for chemically reactive amino acids. Metabolic labeling methods such as BONCAT can therefore be used to screen for previously unknown locally translated or activity-induced proteins. In contrast, TimeSTAMPs are intended to visualize specific proteins of interest and thus are well suited for investigation of any proteins identified in screens by mass spectroscopy or BONCAT.

Preferential incorporation of PSD95 at stimulated synapses

The precise function of activity-induced protein synthesis in synaptic plasticity is still poorly understood. An attractive hypothesis is that proteins synthesized in response to synaptic activity function at activated synapses to promote long-lasting structural changes^{6,45}. This hypothesis predicts that new copies of specific proteins synthesized after synaptic activation will localize to activated synapses. However, an alternative hypothesis is that new protein synthesis replenishes preexisting proteins that are rapidly consumed during synaptic plasticity^{45,46}. If copies of a particular protein synthesized in response to activity are used primarily to replenish global stocks rather than to remodel activated synapses, old copies would be used by the stimulated synapses and new proteins would resupply a dendritic pool to be used later by all synapses. These hypotheses thus make different predictions about fates of newly synthesized proteins.

Our results demonstrate that copies of PSD95 synthesized after localized stimulation preferentially accumulate in stimulated dendritic regions and synapses. This is to our knowledge the first direct observation that copies of a synaptic structural protein synthesized after local dendritic stimulation can preferentially incorporate into stimulated synapses. Because new protein copies are preferentially incorporated at stimulated synapses, our findings support the hypothesis that new synthesis of PSD95 has synapse-autonomous functions and is not solely functioning in global replenishment. Multiple mechanisms have been described that can contribute to the localization of new PSD95 molecules to activated synapses, including local translation¹⁸, activity-induced palmitoylation³⁴ and phosphorylation^{34,38}. PSD95 molecules in PSDs are immobile during baseline activity but exhibit increased exchange between postsynaptic and cytoplasmic locations after LTP or induction of LTD^{39,47}. Preferential accumulation of new copies of synaptic proteins such as PSD95 in stimulated dendritic regions could thus provide synapses undergoing plasticity with proteins to rebuild PSDs or supply fresh copies of proteins that have not yet experienced irreversible post-translational modifications such as proteolysis by calpain⁴⁰. Our finding of high PSD95 levels in stimulated dendritic regions both in synapses and dendritic shafts is consistent with this possibility.

Visualization of new protein copies in synaptic plasticity had previously only been possible for the protein Arc, which is expressed at low levels basally and is strongly transcriptionally and translationally induced after synaptic activity such that induced protein increases can

be attributed to new proteins. In the dentate gyrus of rats, Arc protein levels increase rapidly and specifically in dendritic regions undergoing LTP⁴⁸. However, whether new Arc proteins function to maintain LTP persistence in a synapse-autonomous manner is not yet clear. Arc has a well-characterized function in promoting AMPA-type glutamate receptor removal from synapses in LTD¹⁶, and its requirement in LTP persistence may be due in part to homeostatic removal of glutamate receptors from nonpotentiated synapses. Unlike Arc, which is trafficked with endocytic vesicles away from synapses and is degraded within hours^{16,39}, PSD95 has a half-life of days and a subpopulation is stably bound in the synapse with a persistence of many hours^{11,39}. Once incorporated into specific synapses, new PSD95 could thus conceivably exert long-lasting effects on synaptic function.

Other studies have inferred synaptic incorporation of activity-induced proteins but have not directly demonstrated it. A Dendra2 message tagged with the sensorin 3' UTR is translated near activated synapses in *Aplysia* neurons, suggesting that sensorin itself may be synthesized and used at activated synapses⁴³, but this has not yet been directly confirmed. Preexisting Homer-1a protein, marked by photoactivation of a PA-GFP tag 4 h before synaptic activation, can be recruited specifically to activated synapses in mammalian neurons⁴⁹. However, whether copies of Homer-1a synthesized after synaptic activation target activated synapses has not been studied, and whether Homer-1a synthesis could contribute to the protein synthesis dependence of LTP persistence remains unclear. Fluorescent TimeSTAMP tagging of sensorin or Homer-1a could be used to determine if synapse-specific use of new copies follows their activity-dependent synthesis.

A previous study using local subcellular fluorescence recovery after photobleaching (FRAP) demonstrated that local TrkB stimulation using bead-immobilized BDNF nonspecifically enhanced PSD95-GFP movement throughout the entire dendritic tree without preferential enhancement at the stimulation site³⁰. Local FRAP measurements report replacement rates of total PSD95 in the photobleached location from all sources outside that location. In contrast, we specifically investigated the fates of newly synthesized PSD95 copies. If total protein concentrations are higher than new protein concentrations, then increased accumulation of new proteins may not be apparent when visualizing the total protein population. Furthermore, increased retention of PSD95 at stimulated synapses, for instance, by palmitoylation or phosphorylation^{34,38}, would not increase FRAP and indeed could decrease it if the area of FRAP resides in a larger area of increased retention. The previous study also did not include the native 3' UTR in the PSD95 constructs. Because the 3' UTR mediates mRNA stabilization, dendritic localization and translational induction^{18,20}, its influence on these events would not have been detected.

Ultrastructural pulse labeling of PSD95

Our results demonstrate that visualizing new and old PSD95 proteins by correlated light and electron microscopy with photo-oxidizing TimeSTAMP tags TS:YSOG1 and TS:YSOG2 provides a more complete picture of their localization and environment. By fusing these reporters to PSD95, we found that new and old PSD95 populations exhibited distinct localization patterns both at the cellular and synaptic level. We found PSD95 copies less than 6 h old in dendritic protrusions opposite immature presynaptic termini, and such PSD95 was less abundant in PSDs of mature spines, whereas we preferentially observed older PSD95 populations at mature synapses. This indicates that PSD95 turns over more slowly at PSDs of mature synapses, consistent with previous reports from optical microscopy studies³⁹. New PSD95 populations also exhibited unique synaptic accumulation at each of these

structures. New copies that were less than 6 h old accumulated diffusely in the cytoplasm in a protrusion apposing a vesicle-sparse presynaptic terminus. By contrast, we did not observe copies of PSD95 more than 6 h old in the cytoplasm, and such PSD95 accumulated in dense membrane-bound structures apposing vesicle-rich presynaptic membranes. This could suggest that recruitment of PSD95 to mature postsynaptic sites may require palmitoylation, which has been suggested previously³⁷. Therefore, younger PSD95 molecules do not simply replace older PSD95 populations but exhibit distinct localization and may have distinct functions at growing areas of the neurons.

Without electron microscopy, it would be difficult to distinguish PSD95 labeling at immature versus mature synapses because of the limited contextual information of light microscopy. Super-resolution optical microscopy allows resolution of single targets below the diffraction limit but cannot provide the same contextual information as photo-oxidizing TimeSTAMPs because it is limited by the number of distinct fluorophores that can be imaged simultaneously. It would be difficult to optically label a protein of interest such as PSD95 together with markers required for context, such as membranes, vesicles and microtubules. Electron microscopy inherently includes such context. The only alternative technique for electron microscopy imaging of new versus old copies of a genetically defined protein involves sequential FAsH and ReAsH labeling of tetracysteine motifs⁵⁰. However, the modest singlet oxygen quantum yield of ReAsH makes it much less sensitive than the miniSOG-based approach. The biarsenical dyes also suffer from higher nonspecific background labeling, potential toxicity and difficulty in application to intact tissues and organisms. Photo-oxidizing TimeSTAMPs offer a relatively simple method for ultrastructural resolution of either newer or older copies of a genetically selected protein.

METHODS

Methods and any associated references are available in the [online version of the paper](#).

Note: Supplementary information is available in the [online version of the paper](#).

ACKNOWLEDGMENTS

We thank members of the Tsien and Ellisman laboratories for helpful discussion, especially V. Lev-Ram, S. Adams and T. Deerinck. This work was supported by a US National Institutes of Health (NIH) Pharmacology Training grant (M.T.B.), the US National Science Foundation Graduate Research Fellowships Program (M.T.B.), the Lucille Packard Children's Hospital Pediatric Research Fund (Y.G.), World Class University Program grant R31-2008-000-10083-0 from the Korea Research Foundation of the South Korea Ministry of Education, Science and Technology (N.L.J.), the Howard Hughes Medical Institute and NIH grant 4R37NS027177-23 (R.Y.T.), NIH grant P41GM103412-24 (M.H.E.), NIH grant R01NS076860 (M.Z.L.), and the Burroughs Wellcome Fund (M.Z.L.). M.Z.L. is funded as a Rita Allen Foundation Scholar.

AUTHOR CONTRIBUTIONS

M.T.B. conceived, designed and performed electron microscopy experiments and co-wrote the manuscript. J.Y. designed and validated constructs. Y.G. designed and performed dendritic stimulation experiments. H.J.K. and N.L.J. designed and fabricated microfluidic chambers. X.S. assisted with the study design. M.R.M. assisted with electron microscopy sample preparation and imaging. M.H.E. and R.Y.T. supervised the project and provided advice. M.Z.L. conceived, designed and performed dendritic stimulation experiments, co-wrote the manuscript, and provided supervision and advice.

COMPETING FINANCIAL INTERESTS

The authors declare no competing financial interests.

Published online at <http://www.nature.com/doi/10.1038/nn.3246>.

Reprints and permissions information is available online at <http://www.nature.com/reprints/index.html>.

1. Jung, H., O'Hare, C.M. & Holt, C.E. Translational regulation in growth cones. *Curr. Opin. Genet. Dev.* **21**, 458–464 (2011).
2. Welshhans, K. & Bassell, G.J. Netrin-1-induced local beta-actin synthesis and growth cone guidance requires zipcode binding protein 1. *J. Neurosci.* **31**, 9800–9813 (2011).
3. Phillips, L.L., Pollack, A.E. & Steward, O. Protein synthesis in the neuropil of the rat dentate gyrus during synapse development. *J. Neurosci. Res.* **26**, 474–482 (1990).
4. Sebeo, J. *et al.* Requirement for protein synthesis at developing synapses. *J. Neurosci.* **29**, 9778–9793 (2009).
5. Schuman, E.M., Dynes, J.L. & Steward, O. Synaptic regulation of translation of dendritic mRNAs. *J. Neurosci.* **26**, 7143–7146 (2006).
6. Bekinschtein, P. *et al.* Persistence of long-term memory storage requires a late protein synthesis- and BDNF-dependent phase in the hippocampus. *Neuron* **53**, 261–277 (2007).
7. Bourtochouladze, R. *et al.* Different training procedures recruit either one or two critical periods for contextual memory consolidation, each of which requires protein synthesis and PKA. *Learn. Mem.* **5**, 365–374 (1998).
8. Waung, M.W. & Huber, K.M. Protein translation in synaptic plasticity: mGluR-LTD, Fragile X. *Curr. Opin. Neurobiol.* **19**, 319–326 (2009).
9. Bradshaw, K.D., Emptage, N.J. & Bliss, T.V. A role for dendritic protein synthesis in hippocampal late LTP. *Eur. J. Neurosci.* **18**, 3150–3152 (2003).
10. Abraham, W.C. & Williams, J.M. LTP maintenance and its protein synthesis-dependence. *Neurobiol. Learn. Mem.* **89**, 260–268 (2008).
11. Lin, M.Z., Glenn, J.S. & Tsien, R.Y. A drug-controllable tag for visualizing newly synthesized proteins in cells and whole animals. *Proc. Natl. Acad. Sci. USA* **105**, 7744–7749 (2008).
12. Graf, E.R., Zhang, X., Jin, S.X., Linhoff, M.W. & Craig, A.M. Neurexins induce differentiation of GABA and glutamate postsynaptic specializations via neuroligins. *Cell* **119**, 1013–1026 (2004).
13. Magliery, T.J. *et al.* Detecting protein-protein interactions with a green fluorescent protein fragment reassembly trap: scope and mechanism. *J. Am. Chem. Soc.* **127**, 146–157 (2005).
14. Zhang, C. *et al.* A neuroligin-4 missense mutation associated with autism impairs neuroligin-4 folding and endoplasmic reticulum export. *J. Neurosci.* **29**, 10843–10854 (2009).
15. Bramham, C.R., Worley, P.F., Moore, M.J. & Guzowski, J.F. The immediate early gene *arc/arg3.1*: regulation, mechanisms, and function. *J. Neurosci.* **28**, 11760–11767 (2008).
16. Shepherd, J.D. *et al.* Arc/Arg3.1 mediates homeostatic synaptic scaling of AMPA receptors. *Neuron* **52**, 475–484 (2006).
17. Ehrlich, I. & Malinow, R. Postsynaptic density 95 controls AMPA receptor incorporation during long-term potentiation and experience-driven synaptic plasticity. *J. Neurosci.* **24**, 916–927 (2004).
18. Muddashetty, R.S., Kelic, S., Gross, C., Xu, M. & Bassell, G.J. Dysregulated metabotropic glutamate receptor-dependent translation of AMPA receptor and postsynaptic density-95 mRNAs at synapses in a mouse model of fragile X syndrome. *J. Neurosci.* **27**, 5338–5348 (2007).
19. Todd, P.K., Mack, K.J. & Malter, J.S. The fragile X mental retardation protein is required for type-I metabotropic glutamate receptor-dependent translation of PSD-95. *Proc. Natl. Acad. Sci. USA* **100**, 14374–14378 (2003).
20. Zalfa, F. *et al.* A new function for the fragile X mental retardation protein in regulation of PSD-95 mRNA stability. *Nat. Neurosci.* **10**, 578–587 (2007).
21. Waterhouse, E.G. & Xu, B. New insights into the role of brain-derived neurotrophic factor in synaptic plasticity. *Mol. Cell. Neurosci.* **42**, 81–89 (2009).
22. Kang, H. & Schuman, E.M. A requirement for local protein synthesis in neurotrophin-induced hippocampal synaptic plasticity. *Science* **273**, 1402–1406 (1996).
23. Auerbach, B.D. & Bear, M.F. Loss of the fragile X mental retardation protein decouples metabotropic glutamate receptor dependent priming of long-term potentiation from protein synthesis. *J. Neurophysiol.* **104**, 1047–1051 (2010).
24. Ronesi, J.A. & Huber, K.M. Homer interactions are necessary for metabotropic glutamate receptor-induced long-term depression and translational activation. *J. Neurosci.* **28**, 543–547 (2008).
25. Schratz, G.M., Nigh, E.A., Chen, W.G., Hu, L. & Greenberg, M.E. BDNF regulates the translation of a select group of mRNAs by a mammalian target of rapamycin-phosphatidylinositol 3-kinase-dependent pathway during neuronal development. *J. Neurosci.* **24**, 7366–7377 (2004).
26. Lee, C.C., Huang, C.C., Wu, M.Y. & Hsu, K.S. Insulin stimulates postsynaptic density-95 protein translation via the phosphoinositide 3-kinase-Akt-mammalian target of rapamycin signaling pathway. *J. Biol. Chem.* **280**, 18543–18550 (2005).
27. Taylor, A.M. *et al.* A microfluidic culture platform for CNS axonal injury, regeneration and transport. *Nat. Methods* **2**, 599–605 (2005).
28. Smith, W.B., Starck, S.R., Roberts, R.W. & Schuman, E.M. Dopaminergic stimulation of local protein synthesis enhances surface expression of GluR1 and synaptic transmission in hippocampal neurons. *Neuron* **45**, 765–779 (2005).
29. Wang, K.H. *et al.* *In vivo* two-photon imaging reveals a role of arc in enhancing orientation specificity in visual cortex. *Cell* **126**, 389–402 (2006).
30. Yoshii, A. & Constantine-Paton, M. BDNF induces transport of PSD-95 to dendrites through PI3K-AKT signaling after NMDA receptor activation. *Nat. Neurosci.* **10**, 702–711 (2007).
31. Benarroch, E.E. Metabotropic glutamate receptors: synaptic modulators and therapeutic targets for neurologic disease. *Neurology* **70**, 964–968 (2008).
32. Shu, X. *et al.* A genetically encoded tag for correlated light and electron microscopy of intact cells, tissues, and organisms. *PLoS Biol.* **9**, e1001041 (2011).
33. Chen, X. *et al.* PSD-95 is required to sustain the molecular organization of the postsynaptic density. *J. Neurosci.* **31**, 6329–6338 (2011).
34. Noritake, J. *et al.* Mobile DHHC palmitoylating enzyme mediates activity-sensitive synaptic targeting of PSD-95. *J. Cell Biol.* **186**, 147–160 (2009).
35. Goellner, B. & Aberle, H. The synaptic cytoskeleton in development and disease. *Dev. Neurobiol.* **72**, 111–125 (2012).
36. Toni, N. *et al.* Synapse formation on neurons born in the adult hippocampus. *Nat. Neurosci.* **10**, 727–734 (2007).
37. Bresler, T. *et al.* The dynamics of SAP90/PSD-95 recruitment to new synaptic junctions. *Mol. Cell. Neurosci.* **18**, 149–167 (2001).
38. Kim, M.J. *et al.* Synaptic accumulation of PSD-95 and synaptic function regulated by phosphorylation of serine-295 of PSD-95. *Neuron* **56**, 488–502 (2007).
39. Sturgill, J.F., Steiner, P., Czervionke, B.L. & Sabatini, B.L. Distinct domains within PSD-95 mediate synaptic incorporation, stabilization, and activity-dependent trafficking. *J. Neurosci.* **29**, 12845–12854 (2009).
40. Zadrán, S., Bi, X. & Baudry, M. Regulation of calpain-2 in neurons: implications for synaptic plasticity. *Mol. Neurobiol.* **42**, 143–150 (2010).
41. Bingöl, B. & Sheng, M. Deconstruction for reconstruction: the role of proteolysis in neural plasticity and disease. *Neuron* **69**, 22–32 (2011).
42. Stepanenko, O.V. *et al.* Modern fluorescent proteins: from chromophore formation to novel intracellular applications. *Biotechniques* **51**, 313–314, 316, 318 passim (2011).
43. Wang, D.O. *et al.* Synapse- and stimulus-specific local translation during long-term neuronal plasticity. *Science* **324**, 1536–1540 (2009).
44. Dieterich, D.C. *et al.* In situ visualization and dynamics of newly synthesized proteins in rat hippocampal neurons. *Nat. Neurosci.* **13**, 897–905 (2010).
45. Hernandez, P.J. & Abel, T. The role of protein synthesis in memory consolidation: progress amid decades of debate. *Neurobiol. Learn. Mem.* **89**, 293–311 (2008).
46. Gold, P.E. Protein synthesis inhibition and memory: formation vs amnesia. *Neurobiol. Learn. Mem.* **89**, 201–211 (2008).
47. Blanpied, T.A., Kerr, J.M. & Ehlers, M.D. Structural plasticity with preserved topology in the postsynaptic protein network. *Proc. Natl. Acad. Sci. USA* **105**, 12587–12592 (2008).
48. Steward, O., Wallace, C.S., Lyford, G.L. & Worley, P.F. Synaptic activation causes the mRNA for the IEG Arc to localize selectively near activated postsynaptic sites on dendrites. *Neuron* **21**, 741–751 (1998).
49. Okada, D., Ozawa, F. & Inokuchi, K. Input-specific spine entry of soma-derived Ves1-1S protein conforms to synaptic tagging. *Science* **324**, 904–909 (2009).
50. Gaietta, G. *et al.* Multicolor and electron microscopic imaging of connexin trafficking. *Science* **296**, 503–507 (2002).

ONLINE METHODS

Reagents. Plasmids encoding PSD95 or Arc fused to TimeSTAMP cassettes¹¹ were modified by standard molecular biology techniques including PCR, restriction enzyme digestion and ligation to create new TimeSTAMP variants. New linker sequences were introduced with synthetic oligonucleotides. All subcloned fragments were sequenced in their entirety to confirm successful construction. Full sequences of all plasmids used in this study are available upon request.

The following compounds were obtained from Sigma: bicuculline, CHPG, DHPG, actinomycin D and cycloheximide. Alexa Fluor 647 carboxylic acid succinimidyl ester was from Invitrogen. BILN-2061 and ITMN-191 were synthesized by a contract synthesis company (Acme). BDNF was obtained from Chemicon. Primary antibodies used were mouse monoclonal anti-PSD95 (clone K28/43; Neuromab), mouse monoclonal anti-AU1 (Covance MMS-130R), rat monoclonal anti-HA (clone 3F10; Roche), rabbit anti-Flag (Sigma F7425) and rabbit anti-synapsin (Millipore AB1543P). For immunoblotting, primary antibodies were used at 0.1–0.4 µg/ml and HRP-conjugated goat secondary antibodies (Zymed 626520, 629520 and 656120) at 0.1 µg/ml. For immunofluorescence, primary antibodies were used at 0.5–1 µg/ml and Alexa Fluor 568- and Alexa Fluor 647-conjugated goat secondary antibodies (Invitrogen A-11031, A-21236, A-21244 and A-21247) at 0.5 µg/ml.

Cell culture. All cell culture reagents were obtained from Invitrogen unless otherwise indicated. HEK293A cells (Invitrogen) were cultured in DMEM with 10% v/v FBS, 50 U/ml penicillin and 50 µg/ml streptomycin and transfected with Lipofectamine 2000 (Invitrogen). Hippocampal neurons were dissociated by papain from embryonic day 18 (E18) or postnatal day 0 (P0) Sprague Dawley rats, transfected by Amaxa electroporation (Lonza), cultured in Neurobasal medium with B27 supplement, 2 mM GlutaMAX, 50 U/ml penicillin and 50 µg/ml streptomycin as previously described¹¹. All animal procedures were approved by Institutional Animal Care and Use Committee of the University of California, San Diego or of Stanford University.

Compartmentalized neuronal culture chambers. Silicon wafer masters were made by soft photolithography on two layers of photoresist with patterning provided by two transparency masks created in CAD software and printed on a 20,000 dots-per-inch printer. Polydimethylsiloxane (PDMS) prepolymer and catalyst (Dow Corning) were mixed at a 10:1 ratio and allowed to polymerize on the masters at 70 °C overnight. Blocks were cut out, sterilized and adhered to washed cover glasses, then the channels were coated with poly(D-lysine). Detailed procedures have been previously published²⁷.

Immunoblotting. For analysis of TimeSTAMP cleavage by immunoblotting, HEK293A cells were transfected with Lipofectamine 2000 for 3 h, then transferred to fresh medium without or with BILN-2061. One to two days later, cells were rinsed quickly in Hank's buffered saline solution (HBSS) and immediately lysed in 0.1% boiling sodium dodecyl sulfate (SDS) loading buffer. Lysates were sonicated to shear DNA and then run on NuPage 4–12% Novex Bis-Tris SDS polyacrylamide gels (Invitrogen). Proteins were transferred onto polyvinylidene fluoride membranes (Millipore) by electroblotting, which were then blocked with 10% nonfat dried milk in Tris-buffered saline with 0.1% Tween-20 (TBST), incubated in primary antibody overnight in 5% BSA in TBST at 4 °C, washed in TBST to remove excess primary antibody, incubated in HRP-conjugated secondary antibody in 10% nonfat dried milk in TBST for 45 min at room temperature and finally rinsed 3 times for 10 min each in TBST. Proteins were visualized by chemiluminescence (SuperSignal West Pico Chemiluminescent Substrate, Thermo) and film (Amersham Hyperfilm Blue). For analysis of stimulus-dependent PSD95 synthesis in neurons by immunoblotting, transfected dissociated P0 rat hippocampal neurons were plated and maintained in six-well dishes. After treatment by the desired pharmacological agents, cells were rinsed quickly with HBSS and immediately lysed in boiling SDS loading buffer; then immunoblotting was performed as above.

Immunofluorescence. To quantify effects of TimeSTAMP expression on synaptic density, hippocampal neurons were dissociated, electroporated and plated on washed cover slips coated with poly(D-lysine). Neurons were cultured in the absence of BILN-2061 or in its presence from 4 DIV to 14 DIV. Neurons were fixed by the addition of one culture volume of 8% paraformaldehyde for 15 min

at room temperature, then washed in phosphate-buffered saline (PBS), blocked in PBS with 5% non-immune goat serum and probed for synapsin and HA according to standard procedures. Specificity of secondary antibodies was confirmed in control samples without primary antibody. Cover slips were mounted in Vectashield (Chemicon) and sealed with nail polish. Conditions were randomized and blinded; then images of 7–10 neurons per condition were obtained on a Zeiss Axiovert 200M with a LSM 5 Live confocal scanner, using a ×40 water-immersion lens with numerical aperture (NA) 1.2 and one of the following filter sets: 495/10 nm excitation, 515 nm dichroic, 535/25 nm emission (YFP); 460/20 nm excitation, 515 nm dichroic, 535/25 nm emission (miniSOG); or 540/25 nm excitation, 560 nm dichroic, 595/50 nm emission (mOrange, mKO2 or mCherry). A stack of optical sections with 1,024 × 1,024 resolution at 1-µm intervals through each neuron was obtained and then flattened in a maximum intensity projection. Synaptic density was quantified in a blinded fashion as previously described¹¹. Analysis was performed on an Apple Macintosh notebook computer using the public-domain US National Institutes of Health Image J program (<http://rsb.info.nih.gov/ij/>).

Time-lapse microscopy. To follow fluorescence development of TS:YFP tags in transfected HEK293A cells, cells were cultured and transfected on glass-bottom dishes in DMEM with 10% FBS. One day after transfection, DMEM was exchanged for HBSS with B27. Cells were imaged on a Zeiss Axiovert 200M equipped with a xenon arc lamp, a ×20, 0.7 NA lens, a Photometrics Cascade II 1024 camera and a stage-top environmental chamber with temperature set to 35 °C and humidity to 100%. Images were acquired before and at various times after BILN-2061 addition with exposure times selected to avoid sensor saturation. To plot normalized fluorescence versus time, total background-subtracted fluorescence from individual cells at each time point was measured using ImageJ software and normalized to the maximum value for each cell.

To visualize new synaptic protein synthesis in neurons, dissociated P0 hippocampal neurons were transfected with TimeSTAMP reporters and an mCherry marker by electroporation. They were then cultured in Neurobasal with B27 in glass-bottom dishes or PDMS chambers. Cultures were maintained at 37 °C in 5% carbon dioxide and 100% humidity. Half of the medium was replaced every 2 d. On the day of imaging, medium was exchanged for HBSS with B27. Cells were imaged by epifluorescence on the Zeiss Axiovert 200M as above. They were also imaged on an Olympus IX81 using a ×20, 0.7 NA lens and a FV1000 confocal scanning system. For confocal imaging, the following settings were used: excitation with a 488-nm argon-ion laser line at 10% power and a 559-nm laser diode at 10% power, pinhole 200 µm, scan resolution 1,024 × 1,024 pixels, scanning speed 1 µs per pixel, photomultiplier voltage 700 V, digital gain of 1. In either imaging system, fields including transfected neurons identified by mCherry fluorescence were imaged before and at various times after BILN-2061 addition. A stack of optical sections at 1-µm intervals through each neuron was obtained at each position and time point and then flattened in a maximum intensity projection.

Immunocytochemistry and photo-oxidation for electron microscopy. For conventional immuno-electron microscopy labeling, cells were fixed in 4% paraformaldehyde and 0.1% glutaraldehyde in PBS (0.1 M, pH 7.4) for 30 min, rinsed several times in chilled buffer and incubated in permeabilizing buffer (0.1% Triton X-100 in PBS) for 5 min. Then cells were incubated in primary antibody (monoclonal antibody to HA, 1:1,000, Roche clone 12CA5) in 0.01% Triton X-100 and 5% normal goat serum (NGS) in PBS at 4 °C for 3 h to overnight, with secondary antibody conjugated to biotin (goat anti mouse, 1:1,000) in 5% NGS in PBS at 4 °C for 1–2 h, and streptavidin-HRP (1:100) in 5% NGS in PBS at 4 °C for 1 h, allowing for sufficient washing in 5% NGS in PBS on ice after each incubation. Fluorescent cells were identified and registered by the grid on the cover glass of these dishes. Confocal images of these cells were taken with minimum exposure using a MRC-1024 inverted confocal microscope (BioRad) to identify transfected cells and for correlative light microscopic imaging. Then the buffer was replaced with a solution of 1 mg/ml DAB and 0.001% H₂O₂ in PBS. Cells in the registered grids were monitored under a transmission microscope until a light brown reaction product became visible. The dish was then removed from the microscope and washed in chilled buffer (5 times for 2 min) and post-fixed in 2% glutaraldehyde in 0.1 M PBS on ice for 20 min and then in 1% osmium tetroxide (Electron Microscopy Sciences) in 0.1 M PBS on ice for 30 min. Cells were then washed in chilled buffer twice and rinsed in distilled water and stained with 2%

aqueous uranyl acetate (Ted Pella) for 1 h to overnight at 4 °C. The samples were then dehydrated in a cold graded ethanol series (20%, 50%, 70%, 90%, 100%, 100% and 100% ethanol) for 2 min each, rinsed once in room-temperature anhydrous ethanol and infiltrated in Durcupan ACM resin (Electron Microscopy Sciences) using 1:1 anhydrous ethanol and resin for 30 min, then in 100% resin twice for 1 h each, then into fresh resin and polymerized in a vacuum oven at 60 °C for 48 h. Sample preparation for photo-oxidation was performed as described previously²⁴. Incubation with mersalyl acid (5 mM in cacodylate buffer for 30 min on ice) followed by several rinse steps in chilled buffer before photo-oxidation was added in some experiments to reduce DAB staining of mitochondria.

Electron microscopy. Labeled and imaged areas of embedded cultured cells were identified by transmitted light microscopy. Areas of interest were sawed out using a jeweler's saw and mounted on dummy acrylic blocks with cyanoacrylic adhesive. The cover slip was carefully removed, ultrathin sections were cut using an ultramicrotome, and electron micrographs were imaged using a 1200 TEM (JEOL) operating at 80 keV.

Statistical analysis. Statistical comparisons between two groups for a measure of interest were performed with two-tailed *t*-tests assuming unpaired samples with significance level set at $\alpha = 0.05$. Comparisons between more than two groups for a measure of interest were performed by one-factor ANOVA followed by pair-wise Tukey's tests if ANOVA revealed unequal means at a significance level of $\alpha = 0.05$. Before *t*-tests and Tukey's tests, *F*-tests were first used to reject a null hypothesis of equal variances for a two-tailed distribution with significance level set at $\alpha = 0.05$. If the null hypothesis of equal variances was accepted then Tukey's test (for ANOVA post-*hoc* analysis) or a *t*-test for samples with equal variances was performed; otherwise Dunnett's T3 test (for ANOVA post-*hoc* analysis) or a *t*-test for samples with unequal variances was performed. For analysis of dendritic segment TS:YFP fluorescence or synaptic density, sample numbers were determined by the number of healthy transfected neurons in each condition. For analysis of synaptic TS:YFP fluorescence in chambers, sample numbers were determined by the number of puncta in each segment. Statistical tests were performed in Excel (Microsoft) and Prism (GraphPad).